ELSEVIER

External and internal electrostatic potentials of cholinesterase models

Clifford E. Felder,* Simone A. Botti,*† Shneior Lifson,‡ Israel Silman,† and Joel L. Sussman*§

*Departments of *Structural Biology, †Neurobiology ‡Chemical Physics, Weizmann Institute of Science, Rehovot 76100, Israel*
§Department of Biology, Brookhaven National Laboratory, Upton, NY 11973 USA

The electrostatic potentials for the three-dimensional structures of cholinesterases from various species were calculated, using the Delphi algorithm, on the basis of the Poisson–Boltzmann equation. We used structures for Torpedo californica *and mouse acetylcholinesterase, and built homology models of the human,* Bungarus fasciatus, *and* Drosophila melanogaster *acetylcholinesterases and human butyrylcholinesterase. All these structures reveal a negative external surface potential, in the area around the entrance to the active-site gorge, that becomes more negative as the rim of the gorge is approached. Moreover, in all cases, the potential becomes increasingly more negative along the central axis running down the gorge, and is largest at the base of the gorge, near the active site. Ten key acidic residues conserved in the sequence alignments of AChE from various species, both in the surface area near the entrance of the active-site gorge and at its base, appear to be primarily responsible for these potentials. The potentials are highly correlated among the structures examined, down to sequence identities as low as 35%. This indicates that they are a conserved property of the cholinesterase family, could serve to attract the positively charged substrate into and down the gorge to the active site, and may play other roles important for cholinesterase function.* © *1998 by Elsevier Science Inc.*

Keywords: cholinesterase, electrostatics, electric potential, electrostatic motif

INTRODUCTION

Inspection of the X-ray structure of acetylcholinesterase (AChE, or acetylcholine acetylhydrolase, EC 3.1.1.7) from *Torpedo californica* (*Tc*AChE)[1] revealed that the active site is buried within the enzyme, near the bottom of an approximately 20-Å-long gorge that in places is less than 4 Å wide. It is thought that the substrate acetylcholine (ACh) must travel down this gorge to reach the active site.[1–3] More recently, it has been noticed that *Tc*AChE has a large "dipole moment," calculated to be 500[4] to 1 500 debyes.[5] This would suggest that there is an excess of negative charge in the vicinity of the gorge entrance that might aid in attracting the positively charged substrate toward the gorge. Well before the three-dimensional (3D) structure of AChE was determined, Nolte et al.[6] had already suggested that a high density of negative charge in the vicinity of the active site might serve to attract the substrate toward it.

The concept of a dipole moment can be defined formally only for an electrically neutral entity. This is because, in a charged species, the dipole is no longer a fixed, intrinsic property, but depends on its position in the coordinate system. Nevertheless, there is value in calculating dipole moments even for charged molecules positioned in a consistent way in a common coordinate system, as a measure of the inhomogeneity of the distribution of their partial atomic charges. To distinguish such a dipole from a true dipole moment, we shall call it a position-dependent first moment of charge distribution, $\mu = \Sigma(\mathbf{r}_i q_i)$, where $\mathbf{r}_i$ is the position vector and q_i is the partial charge located on each atom i in the molecule.

Here we examine whether such large first moments are common in cholinesterases (ChEs) in general, and study the relationship between the overall charge distributions and the actual electric potentials, both external and inside the catalytic gorge. The potentials were calculated by solving the Poisson–Boltzmann equation, as implemented in the DelPhi algorithm[7]. Two X-ray structures from the Protein Databank (PDB) were employed, **2ace**[2] for *T. californica* AChE (*Tc*AChE) and **1mah**[8], with the inhibitor fasciculin removed, for *Mus musculus* (mouse) AChE (mAChE). In addition, homology models were prepared for human AChE (hAChE), *Bungarus fasciatus* (snake) AChE (*Bf*AChE), *Drosophila melanogaster* AChE (*Dm*AChE), and human butyrylcholinesterase (hBChE, acylcholine acylhydrolase, EC 3.1.1.8). We also analyze the rela-

Color Plates for this article are on pages 335–337.

Address reprint requests to: J. L. Sussman, Department of Structural Biology, Weizmann Institute of Science, Rehovot 76100, Israel; e-mail: ⟨joel@sgjs3.weizmann.ac.il⟩.

Received 15 January 1998; accepted 6 February 1998.

655 Avenue of the Americas, New York, NY 10010
1093-3263/97/$17.00
PII S1093-3263(98)00005-9

tion between these potentials and a set of conserved, negatively charged residues.

METHODS

Homology models

Homology models of hAChE, *Bf*AChE, *Dm*AChE, and hBChE were constructed using the Swiss-Model server on the World Wide Web[9,10] (URL http://www.expasy.ch/swissmod/SWISS-MODEL.html/). This procedure was chosen because it automatically runs the FASTA[11] and BLAST[12] sequence homology searches against its structural database, and constructs an initial sequence alignment from which it generates an initial model. These initial sequence alignments were later improved by comparison with a multisequence alignment obtained from the program Pileup[13] to produce better models.

The models were constructed using an existing *Tc*AChE structure that Swiss-Model retrieved automatically from its database (**1acj**, a complex of *Tc*AChE with 1,2,3,4-tetrahydro-9-aminoacridine [tacrine] with the tacrine removed), and the appropriate sequences in the Swiss-Prot database, except for *Bf*AChE, whose sequence came from Ref. 14. The final sequence alignments of the model structures with *Tc*AChE are shown in Figures 1–4.

Missing atoms were added to the incomplete side chains of each of these models, using the program WHAT-IF[15], to ensure proper assignment of hydrogens and atomic charges. Each structure was then oriented so that the gorge axis was aligned along the $+z$-coordinate axis. The gorge axis was defined as extending from residue I444 atom CD (I444-CD) to the average of atoms E73-CA, N280-CB, D285-CG, and L333-O (*Tc*AChE numbering)[16]. This orientation is illustrated in the ribbon diagram of Figure 5[17]. While it differs somewhat from that used in previous studies[4], it has the advantage of simplifying the calculation and analysis of properties with respect to the gorge axis. The missing residues 486–489 (HSQE) were added to the *Tc*AChE structure. Throughout this study, the numbering of residues is that of *Tc*AChE[18].

RMS comparisons of the backbone fold

We calculated the root mean square (RMS) deviation of each model from the PDB structure **1acj**, based on the α carbons, using application LSQMAN[19,20]. As shown in Table 1, the average RMS deviations are generally within 1 Å, indicating that the peptide chains of the homology models faithfully follow the *Tc*AChE fold. Table 1 also gives the percent sequence identity and similarity for each model against the **1acj** sequence[18], on the basis of the sequence alignments in Figures 1–4. For evaluations of similarity, we used as sets of similar

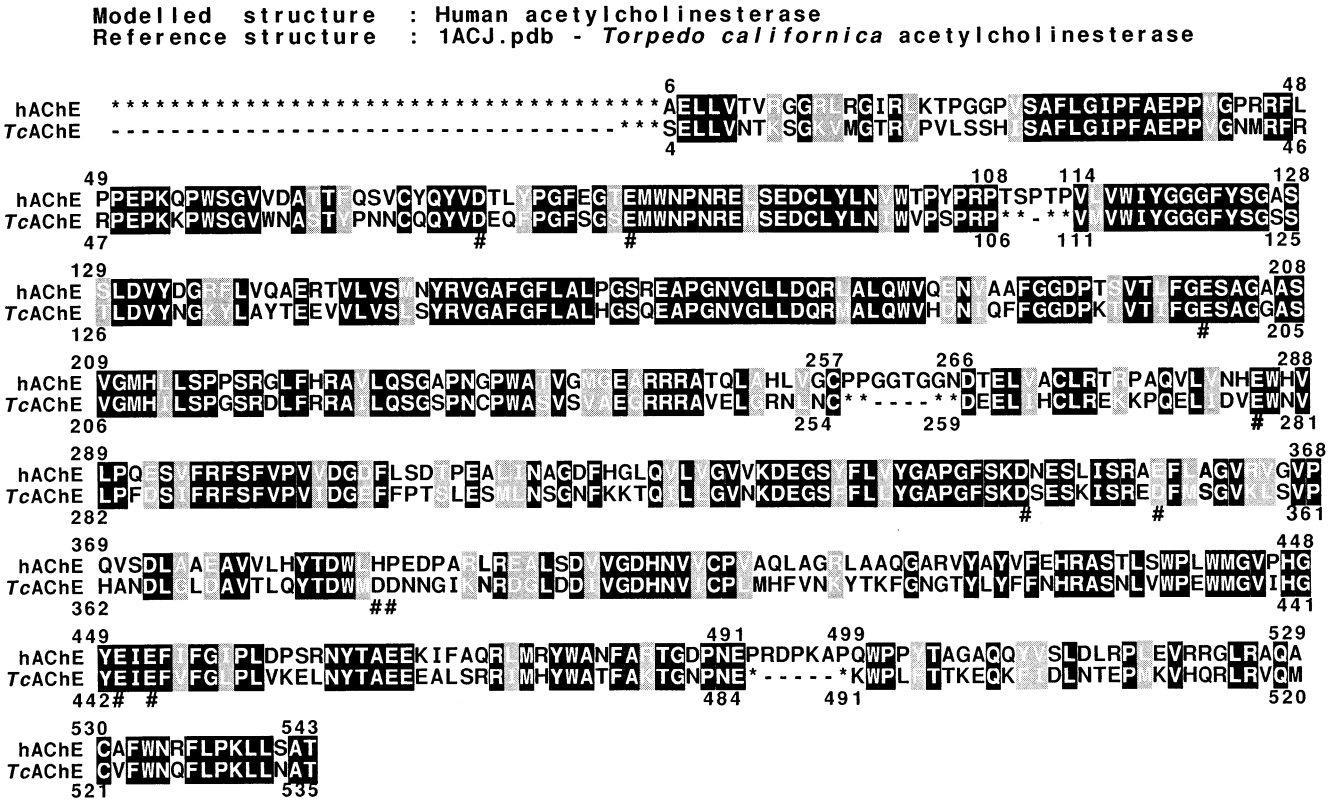

Figure 1. Sequence alignment, in Swiss-Model format, used to construct the homology model of hAChE *relative to structure* **1acj**. *Identical residues are presented against a dark background, and similar residues (A and G; T and S; D and E; K and R; F and Y; N and Q; and I, V, L, and M) are presented against a gray background. Residue positions indicated by an asterisk (*) indicate* **1acj** *residues that were not used in the homology modeling, and dashes (–) mark the locations of missing residues (e.g., locations in the alignment where no residues of a given structure correspond with those given for the other). Hash marks (#) indicate the positions of conserved acidic residues.*

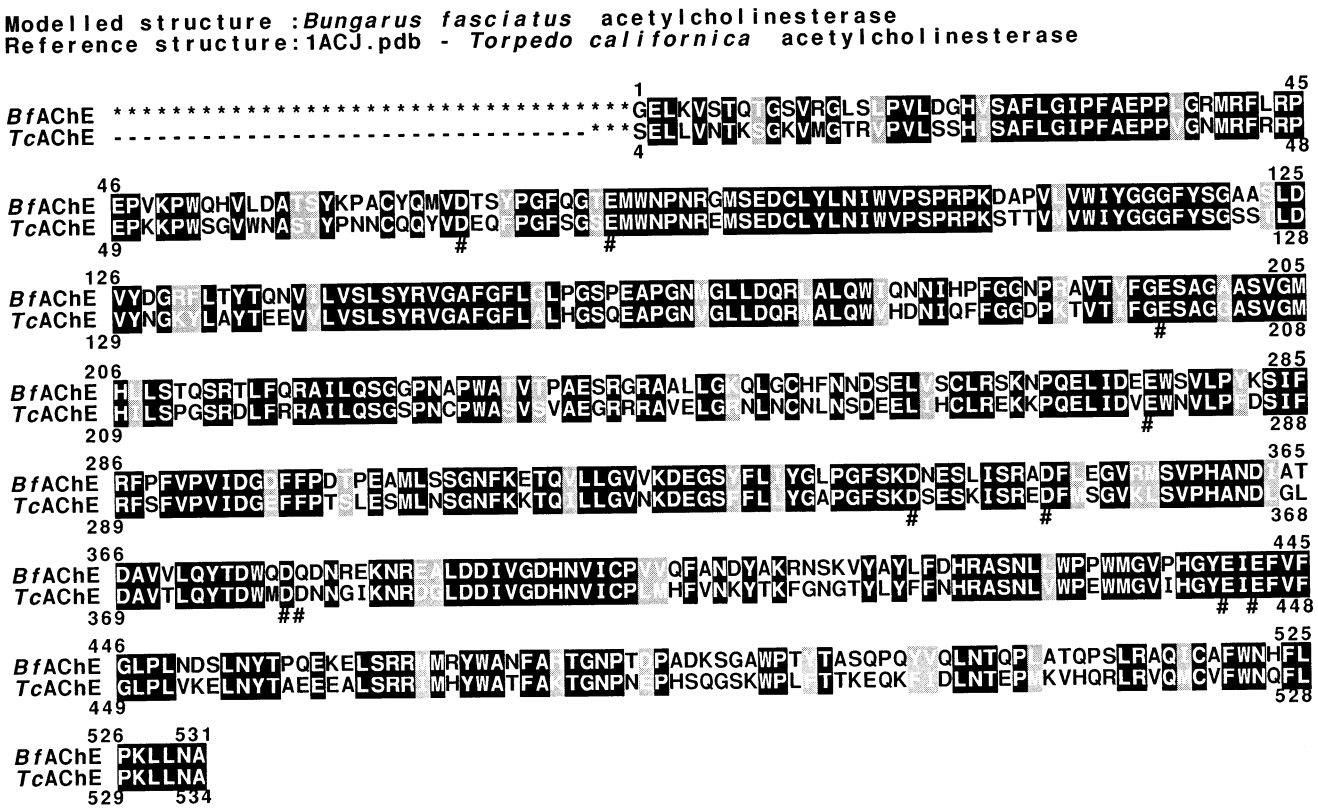

Figure 2. Swiss-Model sequence alignment used to construct the homology model of ***Bf***AChE *relative to* **1acj.**

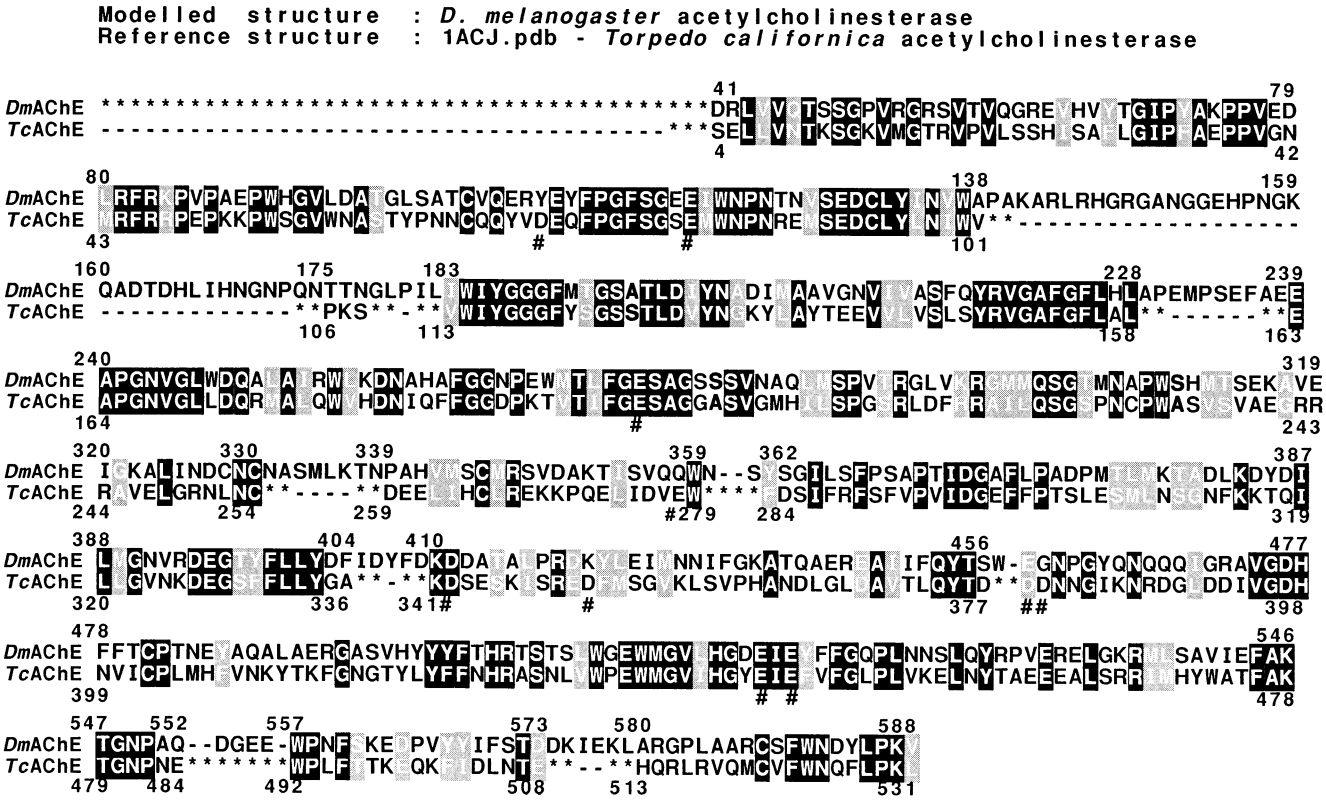

*Figure 3. Swiss-Model sequence alignment used to construct the homology model of Dm*AChE *relative to* **1acj.**

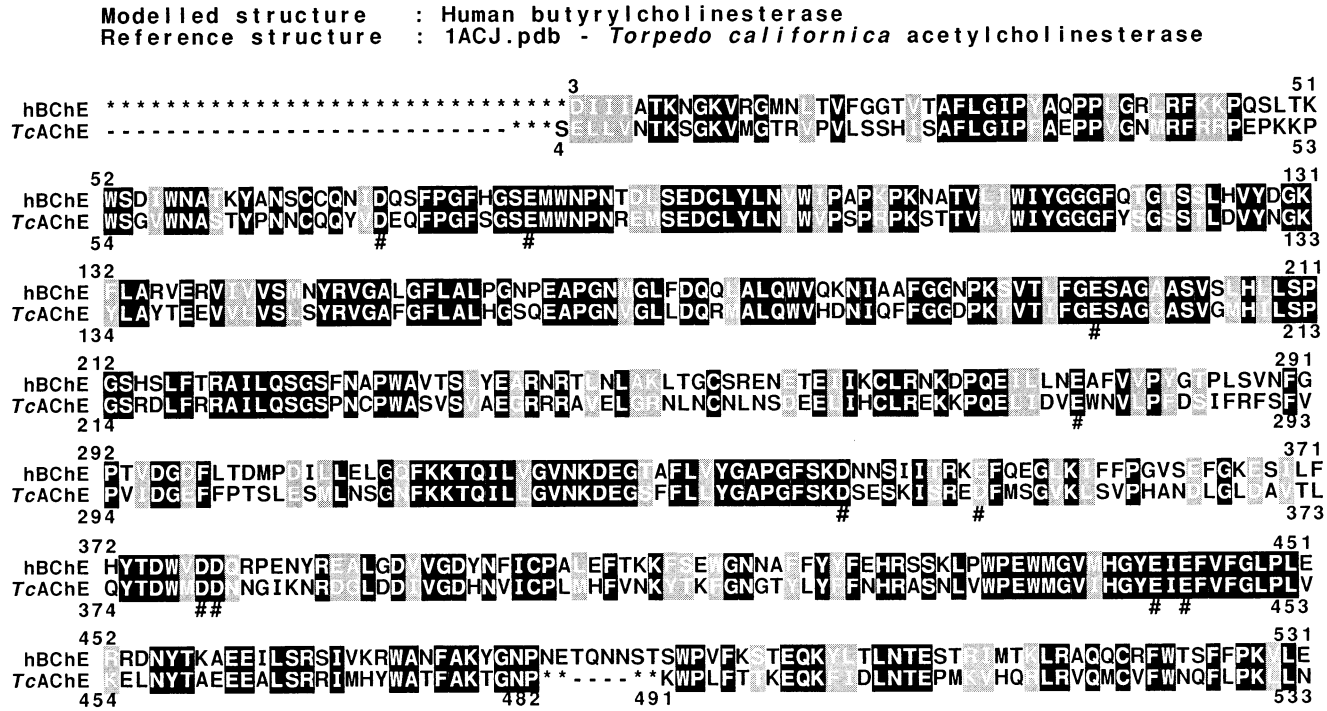

Figure 4. Swiss-Model sequence alignment used to construct the homology model of hBChE *relative to* **1acj.**

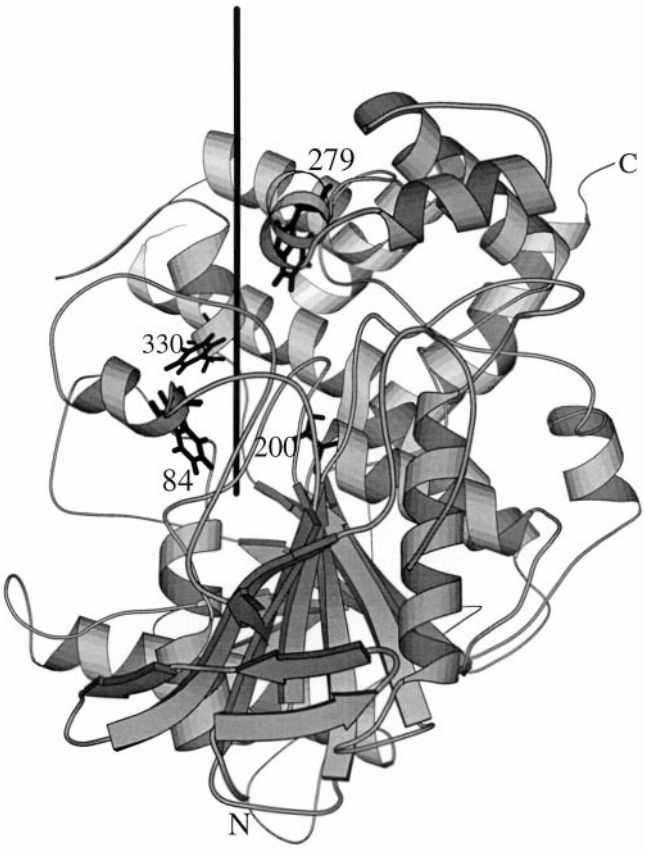

*Figure 5. Ribbon diagram of Tc*AChE. *The diagram was prepared by MOLSCRIPT[17], and shows the orientation employed in Color Plate 1. The gorge axis is denoted by a dark vertical bar, and residues W84, S200, W279, and F330 are drawn as stick figures.*

residues A and G; T and S; D and E; K and R; F and Y; N and Q; and I, V, L, and M (Figure 4 of Ref. 1).

Calculations of position-dependent first moments

The first moments of charge distribution (equivalent to dipole moments; see above) were calculated using the Parse set of partial electric charges on the atoms (optimized specifically for DelPhi to fit data for small molecules; see Ref. 21). Two methods of positioning were used: geometric centering by use of the InsightII DelPhi module[22], and by center of charge, as calculated by GRASP[23].

Calculations of electrostatic potentials by DelPhi

Calculation of electrostatic potentials was performed by solving the Poisson–Boltzmann equation, employing the finite difference method[24] as implemented in the DelPhi algorithm[25]. We employed the Parse partial atomic charges and radii[21], internal and external dielectric constant values of 2 and 80, solvent and ionic probe radii of 1.4 and 2 Å (i.e., closest approach to the molecular surface), respectively, and 0.145 M (physiological) ionic strength. For the electrostatic figures and surface potentials, the easy-to-use application GRASP[23] proved satisfactory. After the electrostatic potentials were calculated, an accessible molecular surface figure, colored according to potential, was prepared, and two files were written, one containing the Cartesian coordinates of the surface points in PDB format, and another containing the corresponding potentials at these points. On the basis of trial profiles of surface point potentials, we established the space containing the external surface points near the gorge entrance to be a cylindrical region starting 25 Å above the gorge base (e.g., atom I444-CD) and between 3.5 and 20.5 Å from the gorge axis. This region was

Table 1. Calculated properties of cholinesterase models, relative to those of *Torpedo californica* acetylcholinesterase

Structure	Percent sequence		Average Cα RMS		Correlation coefficients for:	
	Identity[a]	Similarity[a]	Deviation (Å)[b]	No. of residues[c]	Surface potentials[d]	Gorge potentials[d]
*Tc*AChE[e]	100	100	0.35	528	1.00	1.00
*Bf*AChE[f]	66	75	0.31	524	0.80	0.96
mAChE[g]	58	70	0.89	520	0.89	0.99
hAChE[h]	57	70	0.48	524	0.89	0.99
hBChE[i]	53	69	0.42	525	0.66	0.94
*Dm*AChE[j]	35	48	0.78	508	0.86	0.94

[a] Sequence identity or similarity versus structure **1acj**, according to the sequence alignments given in Figures 1–4, and using as sets of similar residues A and G; T and S; D and E; K and R; F and Y; N and Q; and I, V, L, and M.
[b] Compared with structure **1acj**, as calculated using the program LSQMAN[19,20].
[c] That is, the number of residue pairs LSQMAN used to calculate the RMS deviation.
[d] Compared with the corresponding potentials for the *Tc*AChE structure **2ace**, as determined using the program Linfit[26].
[e] X-Ray structure **2ace** (*Tc*AChE).
[f] Homology model of *Bf*AChE.
[g] X-Ray structure **1mah** (mAChE).
[h] Homology model of hAChE.
[i] Homology model of hBChE.
[j] Homology model of *Dm*AChE.

divided into 1-Å-thick concentric annular sections, e.g., from 3.5 to 4.5 Å from the gorge axis, with mean distance 4 Å, from 4.5 to 5.5 Å, with mean distance 5 Å, etc., as shown in Figure 6, and the average potentials of the surface points in each annulus and in the entire region were calculated.

GRASP is not accurate enough for calculations inside the gorge, which in places is only about 4 Å wide, smaller than the grid spacing in the GRASP potential grid. A commercial version of the program DelPhi[22] was, therefore, employed. This allows a finer grid and greater control over the calculations, e.g., of the nonlinear Poisson–Boltzmann equation, which is not available in GRASP. An initial potential grid with a 35-Å border space, and a grid spacing of about 2.3 Å, was later focused onto a second grid with 10-Å border space and grid spacing of about 1.45 Å (atomic resolution). Finally, we calculated the potential at 1-Å intervals along the gorge axis (as defined above), starting 4 Å above atom I444-CD (*Tc*AChE numbering), using the InsightII DelPhi module. Correlation analyses of the surface and gorge potentials for the specified model were done by a linear regression fit against the corresponding values for the *Tc*AChE structure, using the Linfit algorithm.[26]

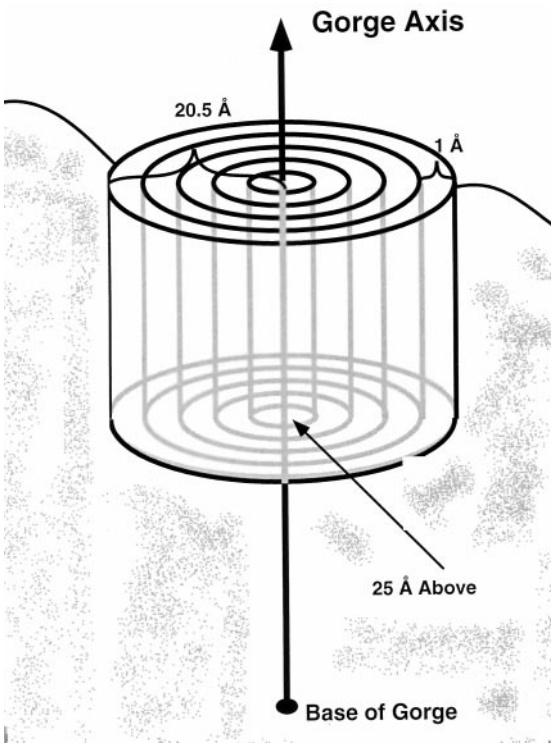

Figure 6. Definition of the annular sections of the accessible molecular surface about the gorge axis.

RESULTS AND DISCUSSION

Sequence similarities and structural RMS deviations

Table 1 presents the sequence identities and similarities versus PDB entry **1acj** for the sequence alignments used to generate the different models. Also presented are the structural RMS deviations of the α carbons relative to those of **1acj**. Most of the sequences have about 55–60% identity, and their corresponding structures have average RMS deviations within 1 Å of that of **1acj**. Our calculated RMS value for mAChE, 0.89 Å, compares well with the value of 0.84 Å calculated in Ref. 8.

Calculated position-dependent first moments of charge distribution

Table 2 shows the calculated net molecular charges, the first moments of charge distribution, and the angles the first-moment vectors make with the gorge axis, for the ChE structures analyzed. All the structures have a rather large moment of

Table 2. Calculated position-dependent first moments of charge distribution (debyes) for cholinesterases and other proteins

Structure	Net charge	Centered geometrically		Center-of-charge centered	
		First moment	Angle with gorge axis (degrees)	First moment	Angle with gorge axis (degrees)
*Tc*AChE	−11	1 666	32	1 676	35
*Bf*AChE	−9	1 688	31	1 639	32
mAChE	−8	1 070	13	1 016	18
hAChE	−10	883	16	948	19
hBChE	−1	1 527	30	1 523	31
*Dm*AChE	−18	1 135	31	1 232	31

800–1 800 debyes, aligned roughly along the gorge axis, and both centering methods agree to within 20%. The calculated value for *Bf*AChE is in fair agreement with the experimentally measured value of 1 000[27]. It can thus be concluded that all the ChEs that we have studied have an asymmetric charge distribution, such that there is an excess of negative charge in the region near the gorge entrance, relative to the far side of the enzyme.

External potentials and those near the gorge entrance

The external potentials of the different ChEs are displayed in Color Plate 1, which shows red (+0.25 kT/*e*) and blue (−0.25 kT/*e*) isopotential surfaces (1 kT/*e* = 25.6 mV). The green arrows represent the directions of the first-moment vectors. The ribbon diagram of *Tc*AChE in Figure 5 defines the view used. In all the structures, the pattern of external potentials reflects strongly the calculated nonhomogeneous charge distributions. In particular, the face of the enzyme leading into the gorge (yellow bar) has a mostly negative potential (red surface), while positively charged regions (blue surface) are mostly on the opposite side.

The surface potentials in the region around the gorge for most of the ChEs are depicted in Color Plate 2, which displays accessible surfaces colored by potential and viewed down the gorge axis. In all the structures, the region around the gorge entrance is red, indicating a negative potential in this area. A close-up view of this region for *Tc*AChE, including a series of isopotential rings (Color Plate 3, top), illustrates clearly the gradually increasing negative potential in this region that could play a significant role in accelerating diffusion of the cationic substrate toward the active site.

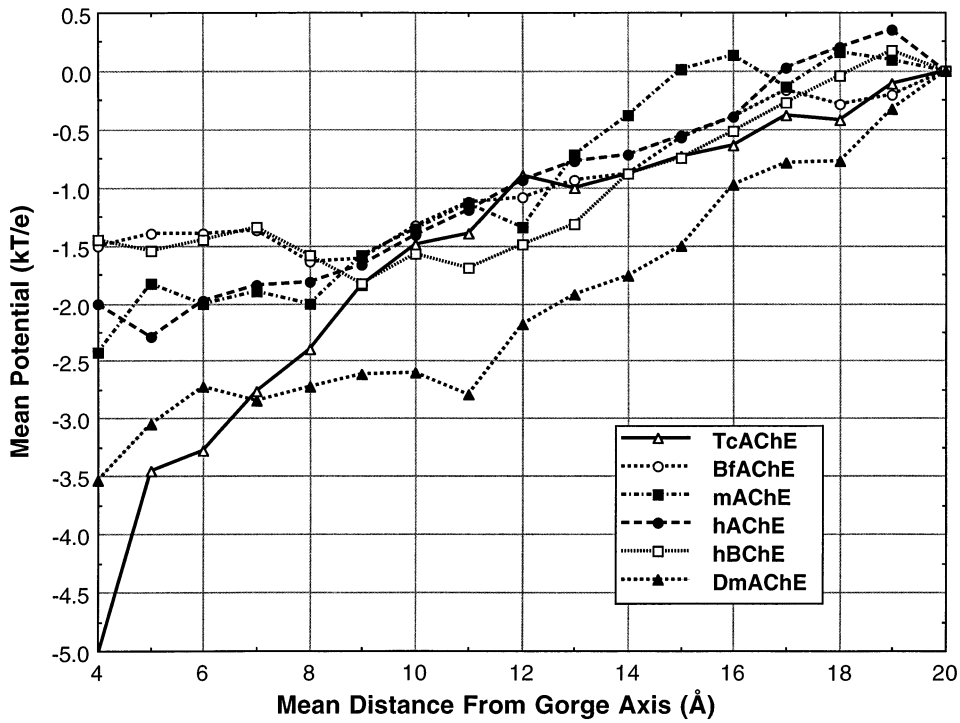

Figure 7. Scaled mean surface potentials in annular sections about the gorge axis in ChE models. These annular regions are defined in Figure 6.

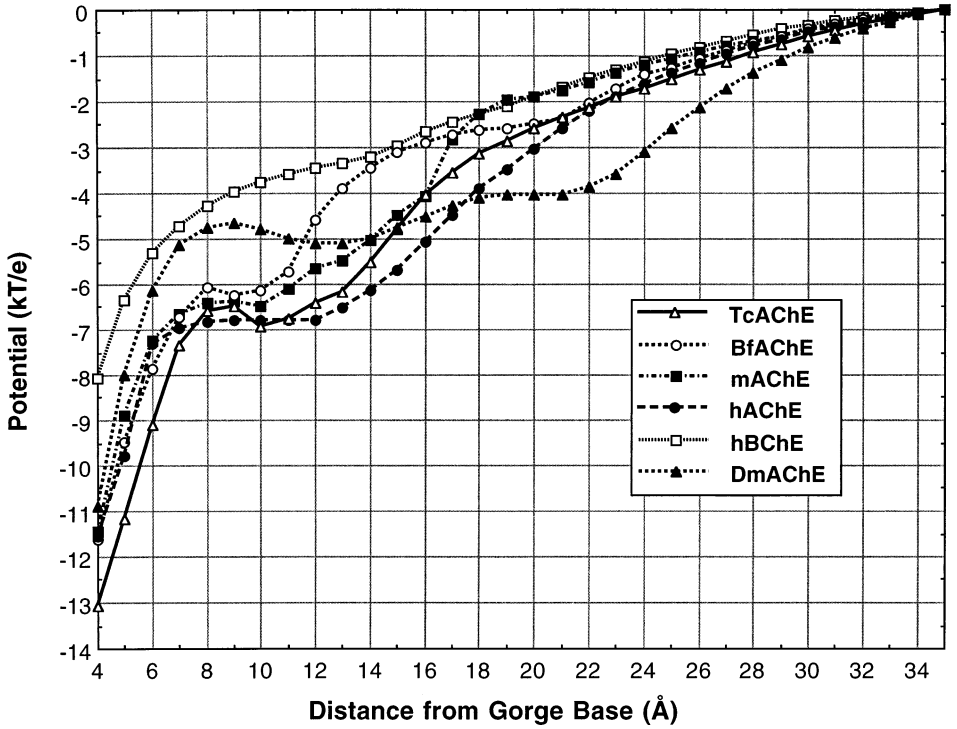

Figure 8. Scaled potentials along the gorge axis in ChE models.

Figure 7 shows the calculated mean potential in a series of 1-Å-thick annular sections out to 20 Å from the gorge axis, for the various ChE structures. They all display a gradually increasing negative potential as the gorge entrance is approached. The correlation coefficients for these curves relative to those for *Tc*AChE are given in Table 1. The average potentials (in kT/*e* units, equal to 25.6 mV or 0.593 kcal mol^{-1} e^{-1}) for the different models over the entire 20-Å cylindrical region are as follows: *Tc*AChE, −2.27; *Bf*AChE, −1.14; mAChE, −1.41; hAChE, −1.14; hBChE, −0.05; and *Dm*AChE, −2.36. All the

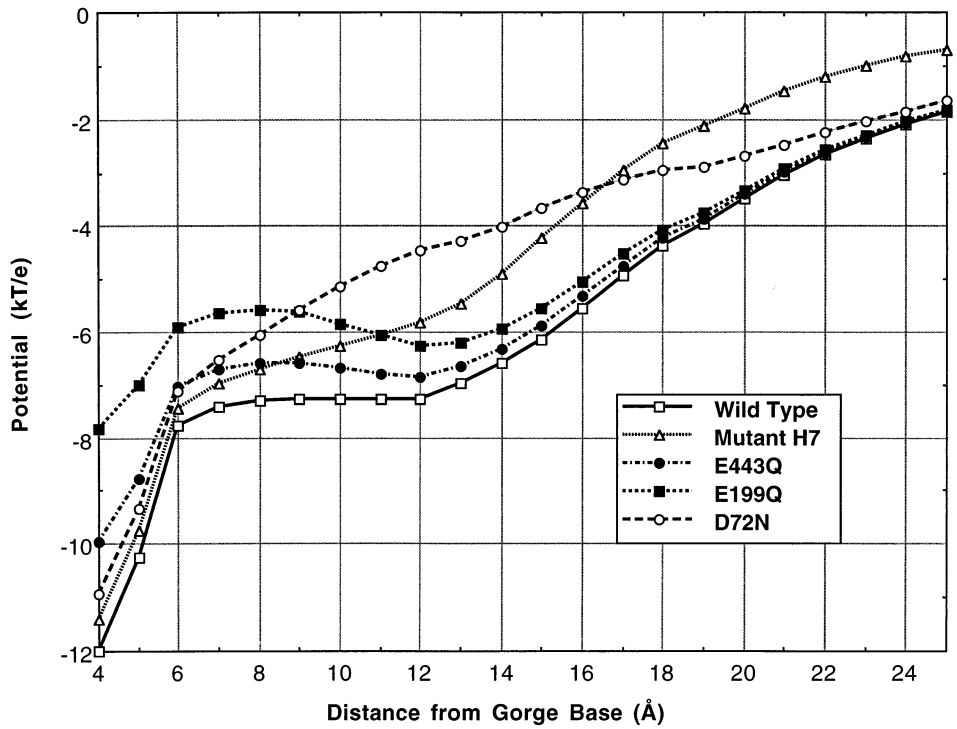

Figure 9. Potentials along the gorge axis in hAChE *mutants.*

Table 3. Conservation of critical acidic residues in the cholinesterase sequence alignments,[a] relative to the *Tc*AChE sequence

Model	D72	E82	E199	E278	D342	D351	D380	D381	E443	E445
*Bf*AChE	*	*	*	*	*	*	*	—	*	*
mAChE	*	*	*	*	*	—	—[b]	—[b]	*	*
hAChE	*	*	*	*	*	(*)	—[b]	—[b]	*	*
hBChE	*	*	*	*	*	(*)	*	*	*	*
*Dm*AChE	—	*	*	—	*	—	(*)	—	*	*

[a] According to the sequence alignments given in Figures 1–4, and a similar alignment for mAChE. The presence of the given residue aligned to that of *Tc*AChE is indicated by an asterisk. An asterisk in parentheses means that glutamate and aspartate have been interchanged, which should not affect the electrostatics. A dash (—) indicates that the residue is not conserved.
[b] In the sequence alignment, these two residues are offset by two positions.

structures show a fairly good correlation to *Tc*AChE, except for hBChE, whose average potential and correlation coefficient are significantly lower. Hence, all the AChEs studied have a common electrostatic pattern or motif[28] around the gorge entrance, while BChE displays a somewhat different pattern. The biological significance of this region of conserved negative potential is under investigation.[29]

Electrostatic potentials along the axis of the catalytic gorge

A slice view through the catalytic gorge of *Tc*AChE (Color Plate 3, bottom, a and b) illustrates clearly that the potential increases gradually as one goes down the gorge, and reaches a maximum near its base. Figure 8 shows a plot of these calculated potentials at 1-Å intervals along the gorge axis, starting 4 Å from the gorge base, for all the models examined. The potentials were scaled such that the potentials 35 Å from the gorge base were set to zero, so as to permit meaningful comparison of the values for the different models. All the AChE models display a similar, gradually increasing negative potential, beginning several angstroms outside the gorge entrance, and continuing down the gorge toward the active site. In an area ~14–8 Å from the base of the gorge, depending on the particular species, the potentials are relatively level, and then drop sharply toward the bottom of the gorge. A similar pattern of potentials for *Tc*AChE was calculated by Wlodek et al.[30] In the case of hBChE the plateau region is essentially absent. Table 1 shows that the gorge potentials, including that for hBChE, have correlations approaching unity versus *Tc*AChE, which is a much smaller degree of variation than that calculated for the external potentials, for the fold or for the sequence similarity. Hence, these potentials are strongly conserved among all the ChEs, and thus may play an important role in drawing the positively charged substrate down the gorge to the active site[4,31,32].

Relation to conserved acidic residues in the sequence alignments

The origin of these conserved potentials can be understood by examining the conservation of key acidic residues in the sequence alignments. Shafferman et al.[33] identified seven surface acidic residues near the gorge (E82, E278, E285, E342, D351, D380, and D381) thought to be primarily responsible for the negative surface potential near the gorge entrance (see also Antosiewicz et al.[16]) Also important is an additional negatively charged residue, D72, located midway down the gorge.[1] Finally, E199 and E443, near the gorge base, together with nearby E445, appear to be primarily responsible for the large negative potential in this region.[30,34] Table 3 shows that 10 of these residues are highly conserved in the sequence alignments of our homology models. In particular, E82, D342, E443 and E445 are conserved among all the models, as is D72 in all but the *Dm*AChE model. E285 is conserved only in hAChE and mAChE, and is not included in Table 3. Hence, the calculated electrostatic properties are a function of certain key acidic residues conserved in the sequence alignment on the backdrop of a common backbone fold. Figure 10 shows the position of these conserved residues within the three-dimensional structure of *Tc*AChE.

As a check, we prepared a second hAChE homology model using version 4 of the program Modeller[35,36], in which four different *Tc*AChE structures and one mAChE structure from the PDB were used together to build the hAChE model. Its

*Figure 10. Ribbon diagram showing the position in the 3D structure of Tc*AChE *of the ten conserved residues listed in Table 3. The black bar denotes the gorge axis.*

calculated surface and gorge potentials are practically identical to those of the original model, with correlation coefficients of 0.97 and 0.99, respectively, against the original hAChE model, and 0.88 and 0.98 against *Tc*AChE, even though the RMS deviation between the two hAChE models was 0.50 Å. Hence our conclusions are valid even if the homology models are only approximate. As a second check, we prepared (by residue replacement) from the first hAChE model a series of mutant models, including E199Q, E443Q, D72N, and the Shafferman et al. H7 mutant[33], in which all seven acidic residues near the gorge entrance listed above were neutralized. Their effects on the gorge potentials are shown in Figure 9, where the H7 mutations affect mainly the potentials in the top half of the gorge, D72N influences the potentials mainly in the middle, at ~12 Å from the base of the gorge, and E199Q and E443Q affect primarily the potential near the base of the gorge. Furthermore, the average surface potential for the H7 mutant was reduced from −1.14 to −0.05 kT/*e* units relative to the wild type (and the patterns of surface and gorge potentials correlated as 0.96 and 0.99 against hAChE WT and as 0.93 and 0.99 against *Tc*AChE). The relatively larger effect of the E199Q and E443Q mutations probably results from these residues being buried within the molecule below the gorge.

We can conclude that the consistent pattern of electric potentials around the entrance to the active-site gorge and within it has its origin in a small number of critical acidic residues that are conserved within highly homologous regions of the sequence alignments, such that they occupy the same key locations in the ChE fold. This explains how structures with sequence identities as low as 35% can have such highly correlated potentials, and suggests that they are important for the functional roles of the ChEs.

ACKNOWLEDGMENTS

The authors thank Charles Millard for valuable comments on the manuscript. This work was supported by the U.S. Army Medical Research Acquisition Activity under Contract No. 17-97-2-7022, the Kimmelman Center for Biomolecular Structure and Assembly (Rehovot, Israel), and the European Union. The generous support of Mrs. Tania Friedman is gratefully acknowledged. I.S. is Bernstein–Mason Professor of Neurochemistry.

REFERENCES

1 Sussman, J.L., Harel, M., Frolow, F., Oefner, C., Goldman, A., Toker, L., and Silman, I. Atomic structure of acetylcholinesterase from *Torpedo californica*: A prototypic acetylcholine-binding protein. *Science* 1991, **253,** 872–879

2 Raves, M.L., Harel, M., Pang, Y.-P., Silman, I., Kozikowski, A.P., and Sussman, J.L. Structure of acetylcholinesterase complexed with the nootropic alkaloid, (–)-huperzine A. *Nature Struct. Biol.* 1997, **4,** 57–63

3 Axelsen, P.H., Harel, M., Silman, I., and Sussman, J.L. Structure and dynamics of the active site gorge of acetycholinesterase: Synergistic use of molecular dynamics simulation and X-ray crystallography. *Protein Sci.* 1994, **3,** 188–197

4 Ripoll, D.R., Faerman, C.H., Axelsen, P.H., Silman, I., and Sussman, J.L. An electrostatic mechanism of substrate guidance down the aromatic gorge of acetylcholinesterase. *Proc. Natl. Acad. Sci. U.S.A.* 1993, **90,** 5128–5132

5 Antosiewicz, J., Gilson, M.K., and McCammon, J.A. Acetylcholinesterase: Effects of ionic strength and dimerization on the rate constants. *Israel J. Chem.* 1994, **34,** 151–158

6 Nolte, H.-J., Rosenberry, T.L., and Neumann, E. Effective charge on acetylcholinesterase active sites determined from the ionic strength dependence of association rate constants with cationic ligands. *Biochemistry* 1980, **19,** 3705–3711

7 Honig, B., Sharp, K.A., and Yang, A.-S. Macroscopic models of aqueous solutions: Biological and chemical applications. *J. Phys. Chem.* 1993, **97,** 1101–1109

8 Bourne, Y., Taylor, P., and Marchot, P. Acetylcholinesterase inhibition by fasciculin: crystal structure of the complex. *Cell* 1995, **83,** 503–512

9 Peitsch, M.C. Protein modelling by e-mail. *Bio/Technology* 1995, **13,** 658–660

10 Peitsch, M.C. ProMod and SwissModel: Internet-based tools for automated comparative protein modelling. *Biochem. Soc. Trans.* 1996, **24,** 274–279

11 Pearson, W.R., and Lipman, D.J. Improved tools for biological sequence comparison. *Proc. Natl. Acad. Sci. U.S.A.*, 1988, **85,** 2444–2448

12 Altschul, S.F., Gish, W., Miller, W., Myers, E.W., and Lipman, D.J. Basic local alignment search tool. *J. Mol. Biol.* 1990, **215,** 403–410

13 Feng, D.F., and Doolittle, R.F. Progressive sequence alignment as a prerequisite to correct phylogenetic trees. *J. Mol. Evol.* 1987, **25,** 351–360

14 Cousin, X., Bon, S., Duval, N., Massoulié, J., and Bon, C. Cloning and expression of acetylcholinesterase from *Bungarus fasciatus* venom—a new type of COOH-terminal domain; involvement of a positively charged residue in the peripheral site. *J. Biol. Chem.* 1996, **271,** 15099–15108

15 Vriend, G.A. WHAT-IF, version 3.0, for Silicon Graphics Indigo, EMBL, Heidelberg, Germany, 1995

16 Antosiewicz, J., McCammon, J.A., Wlodek, S.T. and Gilson, M.K. Simulation of charge-mutant acetylcholinesterases. *Biochemistry* 1995, **34,** 4211–4219

17 Kraulis, P.J. MOLSCRIPT: A program to produce both detailed and schematic plots of protein structures. *J. Appl. Crystallogr.* 1991, **24,** 946–950

18 Schumacher, M., Camp, S., Maulet, Y., Newton, M., MacPhee-Quigley, K., Taylor, S.S., Friedmann, T., and Taylor, P. Primary structure of *Torpedo californica* acetylcholinesterase deduced from its cDNA sequence. *Nature (London)* 1986, **319,** 407–409

19 Kleywegt, G.J. LSQMAN, version 960821/4.7.3, for the Department of Molecular Biology, University of Uppsala, Uppsala, Sweden, 1996

20 Kleywegt, G.J., and Jones, T.A. A super position. *ESF/CCP4 Newslett.* 1994, **31,** 9–14

21 Sitkoff, D., Sharp, K.A., and Honig, B. Accurate calculation of hydration free energies using macroscopic solvent models. *J. Phys. Chem.* 1994, **98,** 1978–1988

22 Biosym. *DelPhi*, version 2.5. Biosym/MSI, San Diego, California 1994

23 Nicholls, A., Sharp, K., and Honig, B. Protein folding and association: Insights from the interfacial and ther-

modynamic properties of hydrocarbons. *Protein Struct. Funct. Genet.* 1991, **11,** 281–296
24 Warwicker, J., and Watson, H.C. Calculation of the electric potential in the active site cleft due to alpha-helix dipoles. *J. Mol. Biol.* 1982, **157,** 671–679
25 Gilson, M.K., Sharp, K.A., and Honig, B.H. Calculating electrostatic interactions in bio-molecules: Method and error assessment. *J. Comput. Chem.* 1988, **9,** 327–335
26 Bevington, P.R. *Data Reduction for the Physical Sciences.* McGraw-Hill, New York, 1969, p. 104
27 Porschke, D., Créminon, C., Cousin, X., Bon, C., Sussman, J.L., and Silman, I. Electrooptical measurements demonstrate a large permanent dipole moment associated with acetylcholinesterase. *Biophys. J.* 1996, **70,** 1603–1608
28 Honig, B., and Nicholls, A. Classical electrostatics in biology and chemistry. *Science* 1995, **268,** 1144–1149
29 Botti, S.A., Felder, C., Sussman, J.L., and Silman, I. *Protein Engineering*, in press
30 Wlodek, S.T., Antosiewicz, J., and Briggs, J.M. On the mechanism of acetylcholinesterase action: The electrostastically induced acceleration of the catalytic acylation step. *J. Am. Chem. Soc.* 1997, **119,** 8159–8165
31 Tan, R.C., Truong, T.N., McCammon, J.A., and Sussman, J.L. Acetylcholinesterase: Electrostatic steering increases the rate of ligand binding. *Biochemistry* 1993, **32,** 401–403
32 Antosiewicz, J., Gilson, M.K., Lee, I.H., and McCammon, J.A. Acetylcholinesterase: Diffusional encounter rate constants for dumbbell models of ligand. *Biophys. J.* 1995, **68,** 62–68
33 Shafferman, A., Ordentlich, A., Barak, D., Kronman, C., Ber, R., Bino, T., Ariel, N., Osman, R., and Velan, B. Electrostatic attraction by surface charge does not contribute to the catalytic efficiency of acetylcholinesterase. *EMBO J.* 1994, **13,** 3448–3455
34 Ordentlich, A., Kronman, C., Barak, D., Stein, D., Ariel, N., Marcus, D., Velan, B., and Shafferman, A. Engineering resistance to "aging" of phosphonylated human acetylcholinesterase: Role of the hydrogen bond network in the active center. *FEBS Lett.* 1993, **334,** 215–220
35 Sali, A., and Blundell, T.L. Comparative protein modelling by satisfaction of spatial restraints. *J. Mol. Biol.* 1993, **234,** 779–815
36 Sanchez, R., and Sali, A. Advances in comparative protein–structure modelling. *Curr. Opin. Struct. Biol.* 1997, **7,** 206–214